A Comparative Study of Hydroxide Adsorption on the (111), (110), and (100) Faces of Silver with Cyclic Voltammetry, Ex Situ Electron Diffraction, and In Situ Second Harmonic Generation

Sarah L. Horswell, Alexei L. N. Pinheiro, Elena R. Savinova,[†] Matthias Danckwerts, Bruno Pettinger,* Mau-Scheng Zei,[‡] and Gerhard Ertl

Fritz-Haber-Institut der Max-Planck-Gesellschaft, Faradayweg 4-6, D-14195 Berlin, Germany

Received June 30, 2004. In Final Form: September 1, 2004

Hydroxide adsorption on the (111), (110), and (100) faces of silver electrodes from mixed NaOH/NaF solution is studied using cyclic voltammetry and in situ second harmonic generation (SHG). Cyclic voltammograms for the three low index silver planes in alkaline electrolytes are for the first time compared. They show two pairs of anodic and cathodic peaks in the potential interval below the equilibrium Ag/Ag_2O potential. These are attributed to the specific adsorption of hydroxide ions followed by submonolayer oxide formation. The differences in the cyclic voltammograms for the (111), (110), and (100) planes are attributed to different (i) work functions, (ii) surface atomic densities, and (iii) corrugation potentials for these surfaces. Ex situ low energy electron diffraction (LEED) and reflection high energy electron diffraction (RHEED) show that disordered adlayers are formed on Ag(111) and Ag(100), in contrast to Ag(110), where ordered structures are produced in the region of the first pair of current peaks. In the region of the second pair of peaks, LEED indicates disordered oxide phases on each crystal plane and RHEED shows the presence of small islands of $c(2 \times 2)$ structure at some potentials on (110) and (100). SHG measurements were performed (i) in the potential scan mode at constant rotational angle and (ii) at constant potential as a function of the rotational angle. The isotropic (for the (111), (110), and (100) planes) and anisotropic (for the (110) and (111) planes) contributions to the SHG intensity were calculated by fitting the experimental data and are discussed in terms of their dependence on the charge density at the interface, on hydroxide adsorption, and on submonolayer oxide formation.

1. Introduction

There has been considerable effort during the past decades aimed at the understanding of the specific adsorption of anions at solid electrodes (see ref 1 and references therein), in particular the thermodynamics and kinetics of adsorption, the origin and the strength of the metal−ion interactions, the extent of charge transfer between the metal and the ion, and the adlayer structures and phase transitions between them.[2] On Ag surfaces, halide adsorption has been the most extensively investigated, with classical electrochemical methods[3,4] as well as ex situ surface science techniques,[5] in situ diffraction techniques,[3k,6] scanning probe microscopies,[5c,7] and extended X-ray absorption fine structure[8] being employed. The cyclic voltammograms (CVs) of Ag(111) and (100) electrodes in the presence of strongly adsorbing halides share some features: a pair of broad peaks, associated with the adsorption/desorption of a disordered layer of anions, followed by one or more pairs of sharper peaks, corresponding to phase transitions to ordered phases. Fluoride adsorption is very weak on all three low index faces, occurring only in low concentrations of[3b] or in the absence of[4] other adsorbing ions, and no ordered structures have been observed.[5a,7c]

Second harmonic generation (SHG) is a useful tool for investigating specific adsorption at the electrode/electrolyte interface. A major advantage of the technique is that it can be applied to study the electrode surface in situ and under potential control. It is complementary to ex situ

* Corresponding author. E-mail: pettinger@fhi-berlin.mpg.de.
[†] Permanent address: Boreskov Institute of Catalysis of the Siberian Branch of the Russian Academy of Sciences, Prospekt Akademika Lavrentieva, 5, Novosibirsk 630090, Russian Federation. E-mail: elensav@catalysis.nsk.su.
[‡] Present address: Department of Physics, National Central University, Jungli, Taiwan 32054.

(1) Magnussen, O. *Chem. Rev.* **2002**, *102* (3), 679.
(2) Wandlowski, Th. In *Encyclopedia of Electrochemistry*; Bard, A. J., Stratmann, M., Eds.; Wiley-VCH: Weinheim, Germany, 2002; Vol. 1, p 383.
(3) (a) Valette, G.; Hamelin, A.; Parsons, R. *Z. Phys. Chem.* **1978**, *113*, 71. (b) Valette, G. *J. Electroanal. Chem.* **1982**, *132*, 311. (c) Valette, G. *J. Electroanal. Chem.* **1983**, *146*, 439. (d) Valette, G.; Parsons, R. *J. Electroanal. Chem.* **1985**, *191*, 377. (e) Valette, G.; Parsons, R. *J. Electroanal. Chem.* **1986**, *204*, 291. (f) Jovic, B. M.; Jovic, V. D.; Drazic, D. M. *J. Electroanal. Chem.* **1995**, *399*, 197. (g) Foresti, M. L.; Innocenti, M.; Kobayashi, H.; Pezzatini, G.; Guidelli, R. *J. Chem. Soc., Faraday Trans.* **1996**, *92* (20), 3747. (h) Innocenti, M.; Foresti, M. L.; Fernandez, A.; Guidelli, R. *J. Phys. Chem. B* **1998**, *102*, 9667. (i) Foresti, M. L.; Innocenti, M.; Forni, F.; Guidelli, R. *Langmuir* **1998**, *14*, 7008. (j) Stevenson, K. J.; Gao, X.; Hatchett, D. W.; White, H. S. *J. Electroanal. Chem.* **1998**, *447*, 43. (k) Wandlowski, Th.; Wang, J. X.; Ocko, B. M. *J. Electroanal. Chem.* **2001**, *500*, 418. (l) Abou Hamad, I.; Wandlowski, Th.; Brown, G.; Rikvold, P. A. *J. Electroanal. Chem.* **2003**, *554−555*, 211. (m) Beltramo, G.; Santos, E. *J. Electroanal. Chem.* **2003**, *556*, 127.
(4) (a) Valette, G. *J. Electroanal. Chem.* **1981**, *122*, 285. (b) Valette, G. *J. Electroanal. Chem.* **1982**, *138*, 37. (c) Bachetta, M.; Trasatti, S.; Doubova, L.; Hamelin, A. *J. Electroanal. Chem.* **1988**, *255*, 237. (d) Valette, G. *J. Electroanal. Chem.* **1989**, *269*, 191. (e) Veggini, F.; Trasatti, S.; Doubova, L. *J. Electroanal. Chem.* **1994**, *378*, 125. (f) Doubova, L.; Trasatti, S. *Electrochim. Acta* **1997**, *42*, 785. (g) Vitanov, T.; Popov, A.; Sevastyanov, E. S. *J. Electroanal. Chem.* **1982**, *142*, 289.
(5) (a) Salaita, G. N.; Lu, F.; Laguren-Davidson, L.; Hubbard, A. T. *J. Electroanal. Chem.* **1987**, *229*, 1. (b) Zei, M. S. *J. Electroanal. Chem.* **1991**, *308*, 295. (c) Yamada, T.; Ogaki, K.; Okubo, S.; Itaya, K. *Surf. Sci.* **1996**, *369*, 321.
(6) (a) Ocko, B. M.; Magnussen, O. M.; Wang, J. X.; Adzic, R. R.; Wandlowski, Th. *Physica B* **1996**, *221*, 238. (b) Ocko, B. M.; Wang, J. X.; Wandlowski, Th. *Phys. Rev. Lett.* **1997**, *79*, 1511.

10.1021/la0483818 CCC: $27.50
Published on Web 11/04/2004

and classical electrochemical techniques, giving valuable additional information on the state of the electrode surface. SHG is a surface specific technique; thus, only the response of the top few layers of atoms of the surface is measured and it has been shown to be very sensitive to small changes at the electrode/electrolyte interface. SHG has been used to study Ag single-crystal electrodes in the absence of adsorbates,[9] in the presence of metal under-potential deposition (upd),[9c] in the presence of halides,[10] in alkaline fluoride electrolytes,[11] as well as at silver electrodes covered by organic films.[12] Changes in the electronic structure of the surface due to adsorbates can be detected in the intensity of the SH light produced and in its anisotropy. The isotropic part of the SH signal is sensitive to the charge and specific adsorption at the interface. The anisotropic part of the signal gives an insight into changes of symmetry on the surface. A varying phase difference between the isotropic and anisotropic contributions to the signal may also indicate changes in surface structure.[10,11d]

Hydroxide adsorption is of particular importance in electrochemistry and electrocatalysis. OH_{ads} is involved in many electrocatalytic processes either as a reactant, the presence of which determines the surface reactivity (oxidation of CO and alcohols on noble metal surfaces), or as an inhibitor (oxygen reduction on noble metal electrodes).[13] In alkaline solution, silver is a good catalyst for oxygen and hydrogen peroxide electrochemical reduction. The issue of the influence of OH_{ads} on the kinetics of oxygen and hydrogen peroxide reduction is rather controversial, some authors suggesting its inhibiting influence on the above reactions on Pt,[13a] Au,[13b,c] and Ag electrodes,[13d–f] whereas Flaetgen et al.[13g] and Eickes et al.[13h] suggest that the formation of OH_{ads} on Ag promotes hydrogen peroxide reduction. Despite its utmost importance, the mechanism of hydroxide adsorption on metal electrodes is still not fully understood. Since OH is a molecular adsorbate, its behavior may be complicated by the O−H bond splitting. Hydroxide adsorption is believed to be an initial step in the complex mechanisms of surface and bulk metal electrooxidation. Among silver single crystals, the (111) plane is the most thoroughly studied.[3j,11,14] The cyclic voltammetry of OH^- on Ag(111) has some similarities with that of halide adsorption at the onset of the adsorption process close to the potential of zero charge (pzc) but shows marked differences at more positive potentials. A number of techniques has been employed in order to investigate the mechanism of OH^- adsorption on Ag(111), including in situ Raman spectroscopy,[14b] ex situ X-ray photoelectron spectroscopy (XPS)[11a] and scanning tunneling microscopy (STM),[14c] and SHG.[11] It has been suggested that electrochemisorption of OH^- initially proceeds without charge transfer from the ion to the metal surface. However, at more positive potentials, OH^- is discharged, giving rise to the formation of surface oxide of the Ag_2O type. The latter has been detected with ex situ XPS.[11a]

To our knowledge, comparative studies of OH^- adsorption on low index silver planes have not been reported yet. This paper presents and compares voltammetry as well as ex situ low energy electron diffraction (LEED)/reflection high energy electron diffraction (RHEED) and in situ SHG results on the three low index planes of Ag in alkaline NaOH/NaF electrolyte.

2. Experimental Section

2.1. Sample Preparation. The Ag(110) and (111) crystals used for the electrochemical and SHG measurements were produced in-house and were oriented to better than 0.5°. The Ag(100) crystal was obtained from Mateck and oriented to better than 0.4°. The surfaces were prepared for measurements by chemical etching with $NaCN + H_2O_2$ solutions (*caution, highly toxic*), followed by hydrogen flame annealing under a gentle Ar stream, using a procedure similar to one described previously.[9a,11a] The crystal was transferred with a drop of ultrapure water to the electrochemical cell and immersed into the Ar-purged electrolyte under potential control at a potential below the pzc. In this way, contact of the crystal with air was kept to a minimum.

For the LEED and RHEED measurements, all three Ag single crystals were obtained from Mateck and oriented to better than 0.4°. The crystal was mounted in the sample holder with tungsten wire, which was also used for resistive heating of the sample. The sample surface was prepared by successive cycles of Ar^+ bombardment ($p = 5 \times 10^{-5}$ mbar, 0.5 keV, ~6 μA cm^{-2}) and annealing to ~800 K. The cycles were repeated until very high quality surfaces were obtained, as confirmed by sharp LEED and RHEED patterns and by the absence of Auger signals due to impurities.

2.2. Electrochemical Measurements. Cyclic voltammetry measurements were conducted using the hanging meniscus configuration in a Kel-F cell fitted with a Luggin capillary. The counter electrode was a Pt wire ring concentric to the working electrode and the reference electrode was Hg/HgO/0.1 M NaOH (+0.165 V vs the normal hydrogen electrode (NHE)). The cell was cleaned with a 1:1 mixture of 25% NH_3 and 30% H_2O_2 and thoroughly rinsed and soaked with ultrapure water. Electrolyte solutions were prepared from NaF (Suprapur, Merck), NaOH (Suprapur, Merck), and Milli-Q water. Milli-Q water was used throughout. The electrolyte used for both cyclic voltammetry and SHG measurements was 0.09 M NaF + 0.01 M NaOH. An in-house-built potentiostat (E-LAB, Fritz Haber Institut) was used to control the electrode potential and a computer to record the CV.

2.3. LEED and RHEED Measurements. The ex situ LEED and RHEED measurements were performed with a setup comprising an ultrahigh vacuum (UHV) chamber (base pressure $<1.5 \times 10^{-10}$ mbar) with a closed sample transfer to an electrochemical chamber (base pressure $<1 \times 10^{-9}$ mbar). The experimental procedures for the LEED and RHEED measure-

(7) (a) Aloisi, G.; Funtikov, A. M.; Will, T. *J. Electroanal. Chem.* **1994**, *370*, 297. (b) Foresti, M. L.; Aloisi, G.; Innocenti, M.; Kobayashi, H.; Guidelli, R. *Surf. Sci.* **1995**, *335*, 241. (c) Sneddon, D. D.; Gewirth, A. A. *Surf. Sci.* **1995**, *343*, 185.

(8) (a) Endo, O.; Kiguchi, M.; Yokoyama, T.; Ito, M.; Ohta, T. *J. Electroanal. Chem.* **1999**, *473*, 19. (b) Endo, O.; Matsumura, D.; Kohdate, K.; Kiguchi, M.; Yokoyama, T.; Ohta, T. *J. Electroanal. Chem.* **2000**, *494*, 121.

(9) (a) Beltramo, G.; Santos, E.; Schmickler, W. *J. Electroanal. Chem.* **1998**, *447*, 71. (b) Shannon, V. L.; Koos, D. A.; Richmond, G. L. *J. Chem. Phys.* **1987**, *87*, 1440. (c) Koos, D. A.; Shannon, V. L.; Richmond, G. L. *J. Phys. Chem.* **1990**, *94*, 2091. (d) Bradley, R. A.; Georgiadis, R.; Kevan, S. D.; Richmond, G. L. *J. Chem. Phys.* **1993**, *99*, 5535. (e) Guyot-Sionnest, P.; Tadjeddine, A. *J. Chem. Phys.* **1990**, *92*, 734. (f) Shannon, V. L.; Koos, D. A.; Richmond, G. L. *J. Phys. Chem.* **1987**, *91*, 5548.

(10) Beltramo, G.; Santos, E.; Schmickler, W. *Langmuir* **2003**, *19*, 4723.

(11) (a) Savinova, E. R.; Scheybal, A.; Danckwerts, M.; Wild, U.; Pettinger, B.; Doblhofer, K.; Schlögl, R.; Ertl, G. *Faraday Discuss.* **2002**, *121*, 181. (b) Danckwerts, M.; Savinova, E. R.; Pettinger, B.; Doblhofer, K. *Appl. Phys. B* **2002**, *74*, 635. (c) Danckwerts, M.; Savinova, E. R.; Horswell, S. L.; Pettinger, B.; Doblhofer, K. *Z. Phys. Chem.* **2003**, *217* (5), 557. (d) Horswell, S. L.; Pinheiro, A. L. N.; Savinova, E. R.; Pettinger, B.; Zei, M. S.; Ertl, G. *J. Phys. Chem. B*, in press.

(12) (a) Santos, E.; Schuerrer, C.; Brunetti, A.; Schmickler, W. *Langmuir* **2002**, *18*, 2771. (b) Santos, E.; Schuerrer, C.; Brunetti, A.; Schmickler, W. *J. Solid State Electrochem.* **2003**, *7*, 567.

(13) (a) Markovic, N. M.; Ross, P. N., Jr. *Surf. Sci. Rep.* **2002**, *45*, 117. (b) Strbac, S.; Adzic, R. R. *J. Electroanal. Chem.* **1992**, *337*, 355. (c) Strbac, S.; Adzic, R. R. *J. Electroanal. Chem.* **1996**, *403*, 169. (d) Sheblovinskii, V. M.; Kicheev, A. G. *Elektrokhimiya* **1980**, *16*, 1653. (e) Honda, M.; Kodera, T.; Kita, H. *Electrochim. Acta* **1983**, *28*, 727. (f) Savinova, E. R.; Wasle, S.; Doblhofer, K. *Electrochim. Acta*, **1998**, *44*, 1341. (g) Flätgen, G.; Wasle, S.; Lübke, M.; Eickes, C.; Radhakrishnan, G.; Doblhofer, K.; Ertl, G. *Electrochim. Acta* **1999**, *44*, 4499. (h) Eickes, C.; Weil, K. G.; Doblhofer, K. *Phys. Chem. Chem. Phys.* **2000**, *2*, 5691.

(14) (a) Jovic, B. M.; Jovic, V. D.; Stafford, G. R. *Electrochem. Commun.* **1999**, *1*, 247−251. (b) Savinova, E. R.; Kraft, P.; Pettinger, B.; Doblhofer, K. *J. Electroanal. Chem.* **1997**, *430*, 47. (c) Shaikhutdinov, S. K.; Savinova, E.; Scheybal, A.; Doblhofer, K.; Schlögl, R. *J. Electroanal. Chem.* **2001**, *500*, 208.

ments have been described in previous publications.[11d,15] RHEED was performed with an incident electron beam energy of 38 keV at grazing incidence (1−2°). This electron beam was also used as the excitation source for the Auger spectroscopy measurements; thus, structural and chemical compositional data were obtained from the same surface region.

Electrochemical measurements were performed in a cell on top of a glass capillary with a platinum wire counter electrode and a Ag/AgCl/KCl(sat.) reference electrode, which was in a separate compartment. All potentials quoted in this text are referred to the Hg|HgO|0.1 M NaOH electrode. The electrolyte concentration was reduced to improve the dry emersion of the sample, to obtain higher quality LEED and RHEED patterns. After characterization in UHV, the crystal was transferred to the electrochemical chamber and rinsed in flowing water for 5 min to remove any salts remaining on the surface, after which it was transferred back and re-prepared with sputtering−annealing cycles.

2.4. SHG Measurements. SHG measurements were conducted in a cell also constructed from Kel-F but with an optical window at the bottom; the amount of glass is thus kept to a minimum. This cell allows simultaneous optical and voltammetric measurements. All optical adjustments were made while the sample was in contact with the electrolyte and under potentiostatic control to ensure that the time between the preparation of the crystal and its immersion was minimal. A Pt wire concentric to the working electrode was used as the counter electrode and the Hg/HgO/0.1 M NaOH electrode as the reference electrode. The cell allows rotation of the sample around its surface normal to measure the SHG anisotropy. Details of the setup have been published elsewhere.[11b]

For the optical measurements, a Nd:YAG laser was used to produce 5 ns laser pulses of ∼150 mJ energy each at the fundamental wavelength 1064 nm and at a repetition rate of 11.5 Hz. The incident and SHG beams were both polarized parallel to the reflection plane; that is, the pp configuration was used. The fundamental beam was blocked after reflection by a colored glass/interference filter setup, and the SH intensity was detected by a photomultiplier tube. The signal was normalized using a reference signal obtained with a photodiode. A Labview software program was used to control the experiment and to process the data. For the anisotropy measurements, the potential of the working electrode was stepped to a fixed value and the SH intensity was recorded as a function of the rotational angle, which was controlled with a step motor. Potentials were increased stepwise in the positive direction and, at the end of the measurement series, the potential was stepped back to its original value in order to check that no irreversible changes had occurred at the electrode surface. For the scan mode measurements, the SH intensity was recorded during a linear potential sweep for several fixed rotation angles.

3. Results and Discussion

3.1. Electrochemical Measurements. Figure 1a presents the cyclic voltammetry curves of the three silver single-crystal surfaces in 0.09 M NaF + 0.01 M NaOH electrolyte. To our knowledge, this is the first time that CVs for all low index silver planes in alkaline electrolytes are compared, although voltammograms of Ag(111)[3j,11a−c,14a] and (100)[14a] in NaOH electrolytes have been reported. The CVs obtained from Ag single-crystal planes prepared by chemical etching and H_2 flame annealing compare very well with those obtained from samples prepared by sputtering−annealing cycles in an UHV environment (see ref 11a,d and also Figure 4). Each curve contains two sets of broad anodic and cathodic current peaks. Earlier studies performed for Ag(111) have shown that both sets of peaks are pH-dependent and shift negatively with the increase in OH^- activity.[11c] In mixed NaOH/NaF electrolytes, the first (more negative) set of peaks exhibits an ∼60 mV/decade shift in the pH interval from 12 to 14[11c] and has been attributed to the specific adsorption of hydroxide. Fluoride also specifically adsorbs on Ag,[4] albeit much more weakly than hydroxide, and dominates on Ag(111) in mixed F^-/OH^- solutions in the pH range from 6 to 10. The second (more positive) pair of peaks on Ag(111) also shows an ∼60 mV/decade shift in the pH interval from 10 to 13 and has been attributed to the discharge of OH^- followed by formation of submonolayer Ag_2O oxide (Ag_2O_{surf}),[11a,c] which will be further discussed below.

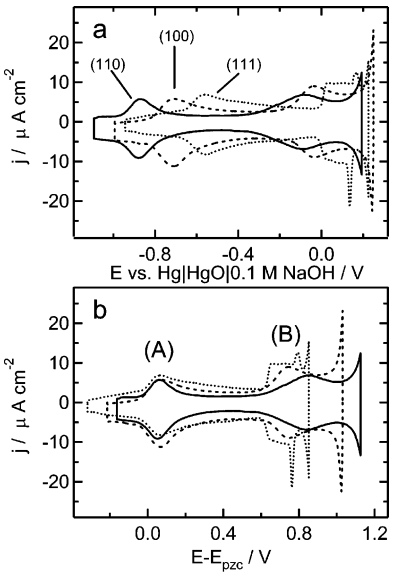

Figure 1. Cyclic voltammetry of Ag(111) (dotted line), Ag(110) (solid line), and Ag(100) (dashed line) in contact with 0.09 M NaF + 0.01 M NaOH: (a) potential referred to Hg/HgO/0.1 M NaOH; (b) potential referred to the respective pzc's (rational potential scale)[4a,b,d]

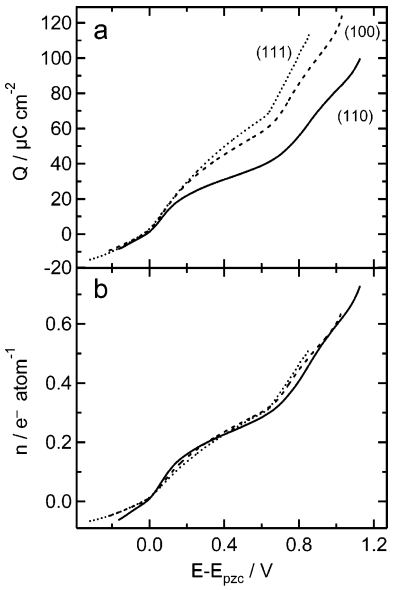

Figure 2. (a) Charge densities of Ag(111) (dotted line), Ag(110) (solid line), and Ag(100) (dashed line) calculated from the voltammograms in Figure 1. (b) Charge densities normalized to surface atomic density (n in e^- per surface atom).

It is instructive to compare the CVs of different Ag crystal faces on a rational potential scale (RPS), which was calculated using pzc's from the literature for the three surfaces in NaF solution.[4a,b,d,g] Figure 1b indicates that the first sets of peaks (labeled A in the figure) and the onsets of the second pairs of peaks (labeled B) coincide. Thus, the difference in the peak positions is related to the difference in the pzc's of the three crystal planes. E_{pzc} ata

(15) Lehmpfuhl, G.; Uchida, Y.; Zei, M. S.; Kolb, D. M. In *Imaging of Surfaces and Interfaces*; Lipkowski, J., Ross, P. N., Eds.; Wiley-VCH: 1999; p 57.

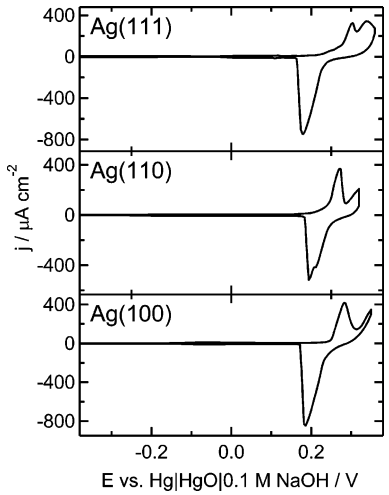

Figure 3. Cyclic voltammetry of (a) Ag(111), (b) Ag(110), and (c) Ag(100) in contact with 0.09 M NaF + 0.01 M NaOH with an extended anodic potential limit.

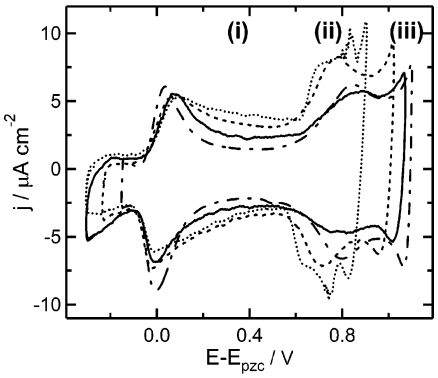

Figure 4. Cyclic voltammetry of UHV-prepared Ag(111) (dotted line), Ag(110) (solid line), and Ag(100) (dashed line) in 5 mM NaF + 1 mM NaOH, plotted on a rational potential scale. For comparison, the CV of Ag(110) in the same solution but prepared by etching and flame annealing is also plotted (dash–dotted line).

metal/electrolyte interface is determined by the work function at a metal/vacuum interface (Φ) and the change in the surface potentials of the metal ($\delta\chi_M$) and the solvent ($\delta\chi_S$) upon their interaction (eq 1):

$$E_{pzc} = \frac{\Phi}{e} + \delta\chi_M - \delta\chi_S \qquad (1)$$

A detailed comparison of published data for E_{pzc} and the work function of Ag single-crystal planes has been made by Trasatti.[16] The dependence of E_{pzc} on the work function is linear with a slope close to 1. This suggests that, despite some differences in the "interfacial parameter" $\delta\chi_M - \delta\chi_S$ between the Ag planes (see discussion in ref 16), the shift of E_{pzc} with Ag atomic density is dominated by the work function. Therefore, the coincidence of the peak positions on the RPS indicates that the onset of OH^- adsorption on Ag is directly related to the work function of the surface.

Although the positions of the voltammetric peaks for low index silver planes on the rational scale are remarkably similar, the shapes of these sets of peaks are different for each surface. The peaks labeled A of the (111) and (100) surfaces are broader with a longer tail toward positive potentials than those of the (110) surface. The set of peaks labeled B of the (111) surface are characterized by a sharp rise in current, followed by a sharp pair of peaks. In contrast, the (110) current rises much more gradually from the onset with a more rounded peak, and the (100) behavior is somewhere between the two. The sharp spikes in the CV of Ag(111) at ~0.78 V (RPS), which were previously attributed to the phase transition from a disordered oxygen adlayer to an ordered surface oxide phase,[11a] are absent in the CVs of the Ag(110) and (100) planes. To gain insight into the different shapes of the CVs, we compare the charge passed during the potential scan. The total charge density transferred through the metal/electrolyte interface (σ_M) was calculated for each crystal by integrating each CV and correcting for the respective charge densities at the potential of the onset of adsorption. The onset potentials were determined by comparing the CVs with those obtained in 0.1 M NaF (not shown). The charge density curves in 0.1 M NaF were determined using literature values of the respective pzc's in 0.1 M NaF.[4a,b,d,g] The charge density curves for the three electrode surfaces in the hydroxide-containing electrolytes are displayed in Figure 2a. At potentials negative of the pzc, the curves of the three surfaces coincide. Although adsorption of OH^- takes place in this potential range, the values of the charge density are small until the onset of the first current peaks. At the potential of the anodic peak labeled A, the total charge density of the (110) surface increases more gradually with potential than that of the other two surfaces, reflecting the shape of the CV. At more positive potentials, the σ_M values for the (111) and (100) surfaces also diverge. This can be explained by normalizing for the atomic density of the three different crystal planes. Assuming surface atomic densities of 1.38×10^{15}, 1.201×10^{15}, and 8.5×10^{14} atoms cm^{-2} for the Ag(111), (100), and (110) planes, respectively, the curves of fractional charge per atom were obtained and are displayed in Figure 2b. These curves can be related to the coverage of the adsorbed hydroxide ions, provided the charge of the diffuse layer is close to zero and that charge transfer between the OH^- adsorbate and the silver surface does not take place. In Figure 2b, the three curves, particularly those of the (111) and (100) planes, are strikingly similar. We thus infer that the differences in OH^- chemisorption on Ag single-crystal planes are related to the different (i) work functions and (ii) atomic densities for these surfaces. It is likely, however, that the surface corrugation potential is also of importance; this will be discussed below.

We now consider the pair of peaks labeled B in the CVs. Comparison of the CVs in OH^- and halide-containing electrolytes proves their marked difference in the potential interval of this pair of peaks. As pointed out in the Introduction, for halides, the peaks are rather sharp, of small charge, and typical of disorder–order transitions. This is different for OH^-, where the second pair of peaks obviously corresponds to a different surface process. In this potential region, ex situ XPS data suggest formation of submonolayer Ag_2O_{surf} oxide, which was detected by the characteristic O1s and $Ag3d_{5/2}$ peaks at 528.2 ± 0.2 and 367.7 eV, respectively.[11a] Transformation of the hydroxide into the surface oxide adlayer presumably occurs according to the following reaction (eq 2):

$$2OH^-_{ads} + 2Ag \rightarrow Ag_2O_{surf} + H_2O + 2e^- \qquad (2)$$

Since a reaction between two anions must be hindered by their repulsive interaction, reaction 2 is likely to proceed in two steps: (2a) discharge of OH^-_{ads} and (2b) interaction

(16) Trasatti, S. *J. Electroanal. Chem.* **1992**, *329*, 237.

of two OH_{ads} species to form adsorbed oxygen or surface oxide.

$$2OH^-_{ads} \rightarrow 2OH_{ads} + 2e^- \quad (2a)$$

$$2OH_{ads} + 2Ag \rightarrow Ag_2O_{surf} + H_2O \quad (2b)$$

The discharge step preceding Ag_2O_{surf} formation is in agreement with results of potential step experiments.[11a] The latter revealed also that surface oxide formation on Ag(111) proceeds by a 2D nucleation and growth mechanism. Hu and Nakatsuji, using the dipped adcluster model, simulated the interaction of two OH species adsorbed at neighboring sites of Ag(100) surfaces and showed that their disproportionation to form adsorbed oxygen and water is favorable for particular adsorbate bondings.[17] Disproportionation of two OH to form surface oxide would also be expected from the inorganic chemistry of silver: it is well-known that Ag(I) forms stable oxide but not hydroxide. We conclude that the coincidence of the onset potentials is a strong indication that the underlying processes are the same for the three silver crystal planes. If, indeed, formation of the surface oxide proceeds through the interaction of two adsorbed OH_{ads}, the reaction activation barrier will be influenced by the surface corrugation potential, which is expected to decrease from Ag(110) to Ag(100) and Ag(111). Calculations by Hu and Nakatsuji[17] suggest that there is little difference in the binding energy of OH to hollow and bridge sites of Ag(111) and only slightly more in the case of (100), which would indicate that the OH_{ads} surface mobility is relatively facile on these two faces. For (110), a substantially larger difference in binding energy between different binding sites was calculated, implying that adsorbate movement is hindered on this face. This may explain the differences in the shapes of the maxima labeled B: the steepest current rise is observed for Ag(111), which has the lowest corrugation potential, the current on Ag(100) increases less steeply, and the current rise is gradual for Ag(110), which has a strongly anisotropic corrugation potential, which hinders adsorbate movement. Additionally, Bange et al.[18] have shown that the OH species on (110) is tilted with the O−H bond oriented along the [001] azimuth. If this is also the case in the electrochemical system, the interaction of two OH adsorbates would be more difficult on the (110) surface than on the other two surfaces.

When the potential is scanned further positive, beyond the anodic peak labeled B in the CV, the current rises steeply for all Ag planes. When the positive limit of the CV is extended above the Ag/Ag_2O equilibrium potential ($E_{eq} = 0.18 - 0.059 \log(a_{OH^-})$ V vs Hg/HgO/0.1 M NaOH (at 25 °C)), the CVs become irreversible, as shown in Figure 3, evidencing the formation of bulk Ag_2O silver oxide in accordance with ref 11a. It should be stressed that, at variance with the OH^- electrosorption process, which is driven by the difference ($E - E_{pzc}$) and is thus shifted for different silver planes on the potential scale, the process of Ag_2O formation is driven by the difference ($E - E_{eq}$) and thus occurs at approximately the same potential values for different Ag crystal planes.

3.2. LEED and RHEED Measurements. Figure 4 shows the cyclic voltammograms in 5 mM NaF + 1 mM NaOH obtained from the three crystals prepared by sputtering−annealing cycles in UHV. The slight distortion of the CVs is a result of ohmic drop due to the low concentration of the electrolyte. For comparison, a CV in the same electrolyte but in a conventional electrochemical cell and using a Ag(110) crystal prepared by etching and flame annealing is also displayed. Figure 5 presents typical LEED patterns of the Ag(111), (110), and (100) surfaces obtained after emersion in region i (between the current peaks) and in region iii (positive potential limit) of the CVs in Figure 4. On Ag(111) and (100), no ordered structures are observed with LEED over the entire potential range, in contrast to the (110) surface. At the Ag(110)/OH^- interface, a range of patterns has been observed with LEED (see Figure 5 and ref 11d) including the following: (i) antiphase domains of $c(2 \times 6)$ structure, which are observed negative of and close to the pzc, (ii) a longer-range ordered $c(2 \times 6)$ structure, which emerges after the first current peak, and (iii) islands of a $c(2 \times 2)$ phase, which develop upon further increase of the electrode potential and consequent OH^- adsorption. At the onset of the current peak labeled B, an abrupt change to a (1×1) pattern was observed.[11d] The (1×1) LEED pattern for Ag(111) obtained at the most positive potential investigated (Figure 5c) shows faint spots with a strong background intensity. This could be due to disordering of the surface, a highly disordered adlayer, or electrolyte deposition as a result of possible wet emersion. Therefore, RHEED patterns were analyzed to determine whether disordering of the surface occurs at positive potentials. Examples of RHEED patterns for the Ag(111) and (100) surfaces are displayed in Figures 6 and 7. In addition, we present intensity profiles across the 2D-integral order rods at the Ag(111) [11$\bar{2}$] and Ag(100) [001] azimuths, to summarize the observations for the different potentials investigated. Figure 8 presents example RHEED patterns of the Ag(110) surface emersed at −0.67 V (region i of the CV) at the [1$\bar{1}$2] and [1$\bar{1}$4] azimuths, in which the Ewald sphere intersects the extra reflections between the integral order beams. The diagrams show the positions of the extra diffraction spots in relation to the Ewald sphere (dotted line) for the displayed patterns. The corresponding intensity profiles across the 2D-integral order rods are also plotted for different emersion potentials. The spacing between the (00) and the nonspecular beams remains

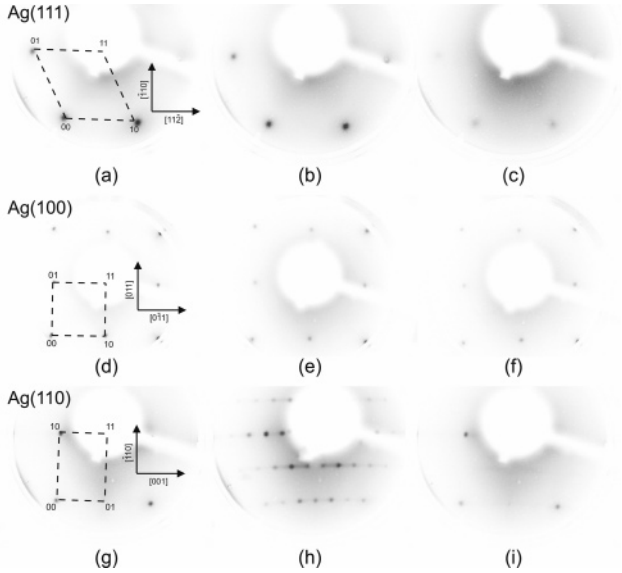

Figure 5. LEED patterns obtained for Ag(111) (top panel), Ag(100) (middle panel), and Ag(110) (bottom panel) surfaces. Left to right: freshly prepared surface, surface after emersion in adsorption region i (between the current peaks), surface after emersion at the positive limit of the CV (region iii).

(17) Hu, Z.-M.; Nakatsuji, H. *Surf. Sci.* **1999**, *425*, 296.
(18) Bange, K.; Madey, T. E.; Sass, J. K.; Stuve, E. M. *Surf. Sci.* **1987**, *183*, 334.

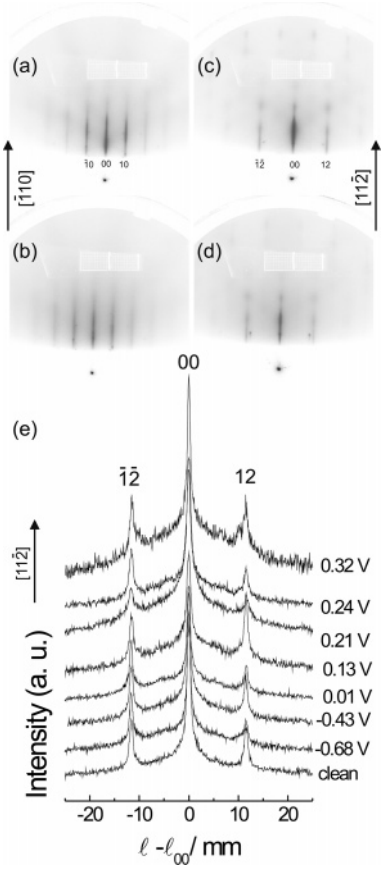

Figure 6. RHEED patterns obtained for Ag(111) in the (a and b) [$\bar{1}$10] and (c and d) [11$\bar{2}$] azimuthal directions. Parts a and c are after emersion in region i, and parts b and d are after emersion in region iii of the CV. (e) Intensity profiles perpendicular to the [11$\bar{2}$] direction of parts c and d for different electrode potentials.

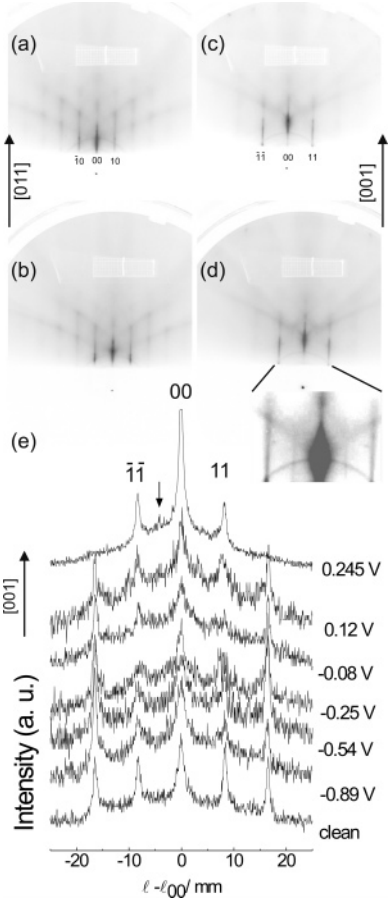

Figure 7. RHEED patterns obtained for Ag(100) in the (a and b) [011] and (c and d) [001] azimuthal directions. Parts a and c are after emersion in region i, and parts b and d are after emersion in region iii of the CV. Part of the pattern in part d is enlarged to show the extra reflection. (e) Intensity profiles perpendicular to the [001] direction of parts c and d for different electrode potentials.

constant throughout the investigated potential range for all three surfaces, at least within the resolution provided by RHEED (~3%). Additionally, the profiles along the reflections (not shown) are unchanged with electrode potential. These observations show that the underlying silver substrates are undisturbed. The RHEED patterns of the (111) surface exhibit some three-dimensional spots due to reflections from crystallites formed upon drying out the electrolyte film on the emersed electrode. This indicates that the bright background of Figure 5c is probably due to these crystallites. A recent scanning tunneling microscopy (STM) study of OH^- adsorption on Ag(111) has revealed the presence of small ordered regions in a 200 mV potential window before the sharp current rise in the CV.[19] This is perhaps reminiscent of the small islands of ordered bromide observed by Guidelli et al. at potentials just negative of the phase transition peak.[7b] The fact that the RHEED patterns do not indicate any ordered adlayer suggests that the structures observed with STM do not have long-range order. Note also that the RHEED results are useful for comparison with SHG rather than the smaller-scale structures because SHG probes macroscopic regions of the surface. RHEED of the (100) surface shows no additional features up to the most positive potential, at which faint streaks corresponding to a $c(2 \times 2)$ pattern are observed. The $c(2 \times 2)$ phase was not visible with LEED, indicating that it is partially distorted. RHEED shows no additional features on Ag(111). The sharp spike in the CV has been previously tentatively assigned to a disorder−order transition.[11a] Although no evidence of an ordered phase was found with RHEED, the potential window between the spike and the sharp rise in current at the positive limit (corresponding to 3D oxide formation) is very narrow. It is possible that the processes giving rise to the latter mask any ordered phase produced by the spike.

In the case of the ordered overlayers on Ag(110), the lattice rods corresponding to the $^1/_2$ order LEED spots intersect the Ewald sphere when the electron beam is in the [1$\bar{1}$2] direction and are thus visible as extra reflections in Figure 8a. The $^1/_6$ order spots are visible in the RHEED patterns of the (110) surface in Figure 8b, because the spots are close enough to the Ewald sphere to intersect it. Examination of the intensity profiles show that, as the electrode potential is made more positive, the $^1/_2$ order spots increase in intensity whereas the $^1/_6$ order reflections remain more or less constant until close to the onset of the second current peak. At the onset, only a $c(2 \times 2)$ pattern remains, as in LEED.[11d] However, RHEED shows that some patches of a $c(2 \times 2)$ phase remain also in the potential region of the second current peak, whereas LEED exhibits only a (1×1) pattern. This suggests that the $c(2 \times 2)$ structure is strongly distorted at these potentials and is likely to be in the form of small islands. The trends of the RHEED intensity profiles are summarized in part e of Figure 8, where the peak heights of the $^1/_6$ order and

(19) Kunze, J.; Strehblow, H.-H.; Staikov, G. *Electrochem. Commun.* **2004**, *6*, 132.

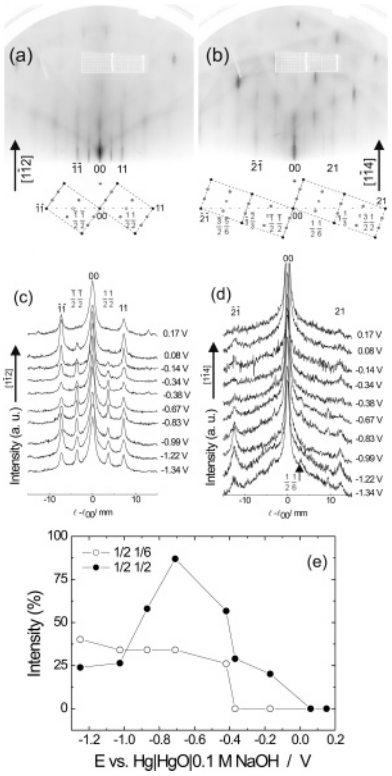

Figure 8. (a and b) RHEED patterns obtained for Ag(110), emersed at −0.67 V, in the [1$\bar{1}$4] and [1$\bar{1}$2] azimuthal directions, respectively. The diagrams indicate the extra reflections observed. (c and d) Corresponding intensity profiles perpendicular to the integral order reflections for different electrode potentials. (e) Peak heights of the fractional order reflections measured from the intensity profiles in parts c and d, plotted as a function of electrode potential.

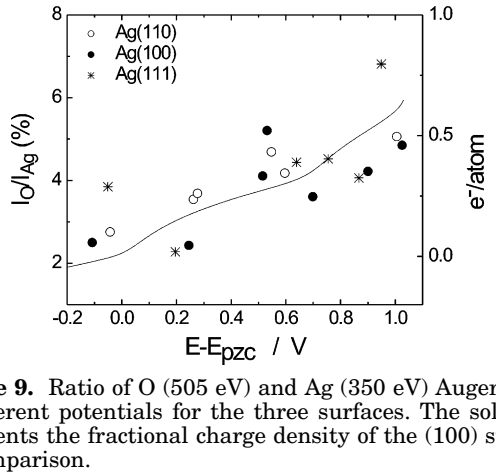

Figure 9. Ratio of O (505 eV) and Ag (350 eV) Auger peaks at different potentials for the three surfaces. The solid line represents the fractional charge density of the (100) surface, for comparison.

$^1/_2$ order reflections are plotted as a function of electrode potential. Note that the $^1/_2$ order reflection is a combination of both $c(2 \times 6)$ and $c(2 \times 2)$ patterns.

Figure 9 represents Auger peak ratios (I_O/I_{Ag}) as a function of potential. For comparison, the fractional charge density as taken from Figure 2b is also plotted. Although the scatter is high, due to the low oxygen signals obtained (Auger is inherently insensitive to oxygen), a clear trend for an increase in oxygen coverage can be discerned from the data, in agreement with the increase in fractional charge density. This result shows that the lack of order observed from some of the diffraction patterns is not due to the desorption of weakly bound species upon emersion and transfer to the UHV environment but simply due to the presence of a disordered adlayer.

OH adsorbed in UHV forms ordered $(1 \times m)$ structures on Ag(110),[18,20] $c(2 \times 2)$ patterns on Ag(100),[21] and no ordered adlayers on Ag(111).[21] The differences between the OH adlayer structures on (110) produced by UHV methods and by electrochemical adsorption for (110), and the absence of ordered structure for electrochemically adsorbed OH^- on (100) may be explained by the lower coverage of OH^- and/or the presence of coadsorbed anions (F^-) and cations (Na^+) on the emersed electrode (the latter are expected in the case of superequivalent OH^- adsorption).

Our diffraction patterns point to some similarities as well as some differences compared with the adsorption of halides on Ag low index planes. At negative potentials, ex situ LEED and in situ STM have shown that Br^- and Cl^- adsorb randomly on the (111) surface, and in situ surface X-ray scattering (SXS) has shown that Br^- and Cl^- adsorb randomly on the (100) face. Therefore, it is not surprising that, at negative potentials and low coverages of OH^-, disordered adsorption occurs. To our knowledge, structural information for halides on Ag(110) has not yet been reported. However, our preliminary LEED/RHEED results show ordered structures of Br^- and Cl^- on Ag(110) at negative potentials. Similarly, OH^- forms ordered overlayers. The anisotropy of the (110) surface apparently induces ordering in the adlayer due to the stronger corrugation potential. In contrast with halides, OH^- does not undergo a phase transition to an ordered phase at more positive electrode potentials. It is likely that, instead, the OH^- is discharged and transformed to O_{ads}, as discussed above. The O adlayer is apparently disordered in the electrochemical environment, despite the fact that ordered O adlayers have been reported in the UHV environment.[22] This is perhaps due to the growth of the oxide via an island formation mechanism, as was previously proposed for Ag(111) in alkaline fluoride electrolytes.[11a,14c]

3.3. Second Harmonic Generation Measurements. SHG anisotropy was measured for the Ag(111), (110), and (100) surfaces in the potential intervals of the CVs displayed in Figure 1a. The shapes of the curves are described by the following phenomenological equation:[23]

$$I^{pp}_{SHG} = |A + B\cos\phi + C\cos 2\phi + D\cos 3\phi|^2 \quad (3)$$

where I^{pp}_{SHG} is the SH intensity, A is the isotropic contribution to the signal, and B, C, and D are the anisotropic contributions of 1-, 2-, and 3-fold symmetry, respectively. All the amplitudes are, in general, complex quantities. SHG measurements were performed (i) in the potential scan mode at constant rotational angle and (ii) at constant potential as a function of the rotational angle. The scan mode results for the three Ag planes compare with the corresponding angles in the anisotropy data very well (not shown but see ref 11a for (111) and ref 11d for the (110) plane), thus justifying that the changes in the

(20) (a) Canepa, M.; Cantini, P.; Mattera, L.; Narducci, E.; Salvietti, M.; Terrini, S. *Surf. Sci.* **1995**, *322*, 271. (b) Canepa, M.; Cantini, P.; Narducci, E.; Salvietti, M.; Terrini, S.; Mattera, L. *Surf. Sci.* **1995**, *343*, 176.

(21) Klaua, M.; Madey, T. E. *Surf. Sci. Lett.* **1984**, *136*, L42.

(22) (a) Engelhardt, H. A.; Menzel, D. *Surf. Sci.* **1976**, *57*, 591. (b) Rovida, G.; Pratesi, F. *Surf. Sci.* **1975**, *52*, 542. (c) Albers, H.; van der Wal, W. J. J.; Gijzeman, O. L. J.; Bootsma, G. A. *Surf. Sci.* **1978**, *77*, 1.

(23) (a) Sipe, J. E.; Moss, D. J.; van Driel, H. M. *Phys. Rev. B* **1987**, *B35*, 1129. (b) Pettinger, B.; Bilger, C.; Lipkowski, J.; Schmickler, W. In *Interfacial Electrochemistry*; Wieckowski, A., Ed.; Marcel Dekker: New York, 1999; p 373.

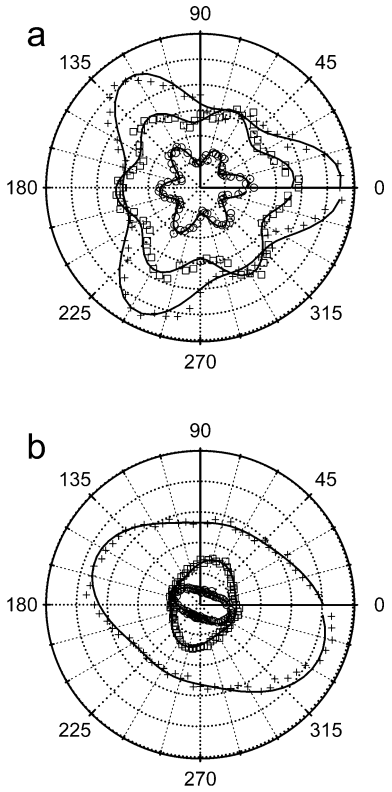

Figure 10. Examples of anisotropy curves in 0.09 M NaF + 0.01 M NaOH: (a) Ag(111) −0.8 V (circles), −0.3 V (squares), +0.1 V (crosses); (b) Ag(110) −1.1 V (circles), −0.6 V (squares), −0.2 V (crosses). The potentials have been chosen such that they correspond to similar potential values on the rational scale. Symbols represent data points and solid lines the best-fit curves calculated using eq 3. Rotational angles are labeled in degrees.

anisotropy patterns can be directly related to the CVs. SHG anisotropy data will be described for each crystal plane in turn, and the final section of the paper will compare the three surfaces.

Ag(111). Figure 10a presents selected anisotropy curves for Ag(111) surfaces at different electrode potentials. As expected, the (111) surface displays 3-fold symmetry. In the figure, the symbols represent the data points collected and the solid lines represent the best-fit lines calculated from eq 3. Calculated fits of anisotropy curves over the whole potential range studied are given in a 3D plot in Figure 11. At negative potentials, six approximately equal maxima are observed, which increase in intensity in the interval of the first voltammetric peak (hydroxide adsorption). When the potential enters the interval of the second voltammetric peak (submonolayer surface oxide formation), a drastic change occurs and three large and three small maxima are formed.

For the (111) surface, the B and C terms, as determined from the fitting procedure, are small and eq 3 reduces to the following:

$$I^{pp}_{SHG} = |A + D\cos 3\phi|^2 = |A|^2 + |D|^2\cos^2 3\phi + 2|A||D|\cos 3\phi\cos\psi \quad (4)$$

where ψ is the phase difference between the (complex) A and D terms. Figure 12 displays the isotropic (A) and anisotropic (D) terms calculated from fitting the anisotropy results to eq 3 as a function of electrode potential. The rational potential scale is used to facilitate comparison between crystal planes. Although the actual phase is not measured in these experiments, the difference between

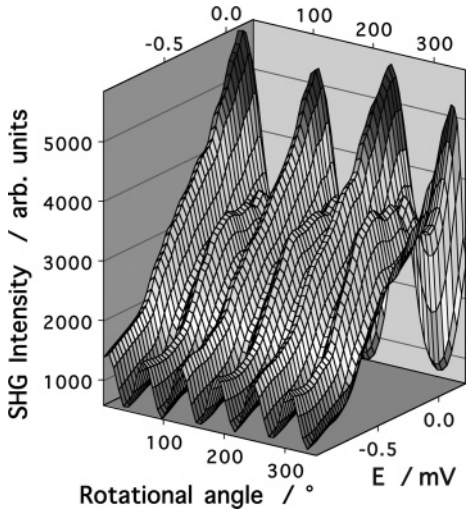

Figure 11. Plot of SH intensity as a function of rotational angle and potential for the Ag(111) surface.

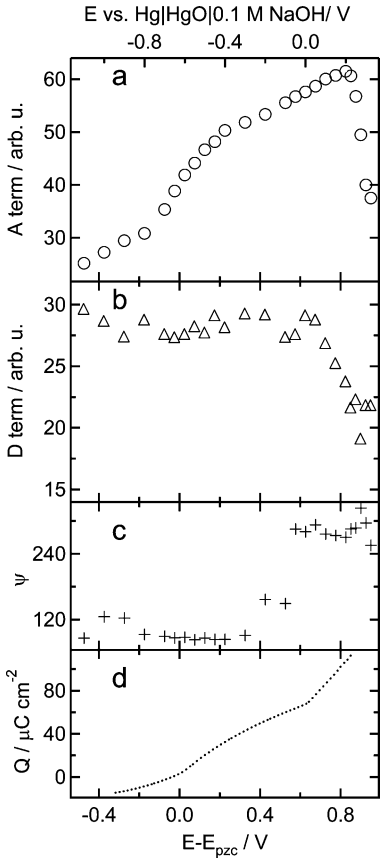

Figure 12. Ag(111) (a) isotropic A term, (b) anisotropic D term, and (c) phase difference (ψ) as a function of electrode potential on the rational scale. Data calculated from anisotropy curves in Figure 11. The dotted line in part d is the charge density.

the phases (ψ) can be obtained from the complex A and D terms, and is also plotted in Figure 12. The dotted curve shows the charge density. The isotropic A term for the (111) crystal comprises susceptibility tensor elements in the z-direction, namely, χ_{zzz}, χ_{zxx}, and χ_{xzx}, which explains its increase in the potential interval from −0.4 to ∼0.8 V RPS, as the potential drop across the double layer increases. The drop in the A term at positive potentials coincides with the current rise at the positive limit of the CV and is obviously related to bulk surface oxidation as the electrode potential approaches the reversible Ag/Ag_2O potential. This is apparently due to the lower polarizability

of oxidized silver compared with the bare metal.[9e,11a,c,24] The anisotropic contribution to the SH signal provides information on the symmetry of the silver surface. The latter determines which elements of the susceptibility tensor contribute to the SH response.[23] In the case of Ag(111), the contribution to the anisotropic part of the signal is from the element χ_{xxx}; therefore, the *D* term arises from in-plane interactions only. The *D* term shows little variation with potential until ~0.7 V RPS, just before the sharp spike in the CV, at which point it rapidly drops. At this potential, ex situ XPS evidences formation of submonolayer Ag_2O and ex situ STM shows the appearance of islands on the surface, which have been attributed to islands of surface Ag_2O oxide.[11a,14c] It has thus been concluded that the disorder on the surface corresponds to the formation of 2D islands of surface Ag_2O oxide and that the fast growth of this disorder is reflected in the drop of the *D* term. It has been suggested that it is a transition to the surface oxide phase which gives rise to the spikes at ~0.78 V RPS in the CV of Ag(111).[11a]

The phase difference between the *A* and *D* terms (ψ) is nearly constant in a large potential interval from −0.4 to +0.5 V RPS, but it then rises abruptly to reach a new value (~120° higher), which is then again constant. The rise in the phase occurs at around the onset of the current peak labeled B in the CV. In a number of previous publications, it has been pointed out that processes at solid/liquid interfaces are reflected in changes of the phase (ψ). Beltramo et al.[10] have shown that phase transitions between different adlayer structures of halide ions specifically adsorbed on single-crystal Ag electrodes induce changes in ψ. However, probing Ag(111) emersed from NaF/NaOH electrolyte with LEED did not reveal any ordered adsorbate structure (see section 3.2). We note that, in the case of slightly acidic (pH 5.8) NaF electrolyte, where Ag dissolution rather than oxide formation occurs at positive potentials, ψ stays nearly constant until the onset of Ag dissolution. The distinct changes in ψ observed in the presence of OH at the onset of the current peak labeled B point to a substantial change in the electronic structure of the interface, which according to the above-mentioned XPS data occurs upon transformation of hydroxide into a surface oxide adlayer. It is the abrupt change in the phase ψ which leads to the drastic alteration of the SH pattern from Ag(111) upon passing from the interval of the first to the second voltammetric peak.

Let us now analyze the SH response of the Ag(111) surface in the potential interval from −0.2 to 0.4 V RPS, which corresponds to the specific adsorption of hydroxide ions. The *A* term roughly follows the charge, showing, however, some deviation from linearity, which increases as the potential enters the region of surface oxide formation. It is notable that neither ψ nor the *D* term changes in this potential interval. Comparison of the SHG data in NaF/NaOH and slightly acidic (pH 5.8) NaF electrolyte shows that the overall behavior of *A*, *D*, and the relative phase is remarkably similar in the potential interval where no faradaic processes (i.e., Ag dissolution or oxidation) occur.[11c] An increase of the SH intensity with the charge density at the interface is in accordance with the parabolic model, which predicts that the SH intensity is proportional to the square of the static electric field E_{DC} at the interface, in the free electron approximation.[9e,25] Since E_{DC} is not exactly known, quantitative verification of the parabolic model is complicated. Since

$$E_{DC} = \frac{\Delta\varphi}{d} \propto \frac{\sigma_M}{\epsilon}$$

(where $\Delta\varphi$ is the potential drop across the double layer, *d*, its thickness, and ϵ, the dielectric constant), a strictly linear correlation between the *A* term and either σ_M or $\Delta\varphi$ should not be expected. The correlation between the *A* term and σ_M in the potential range of OH^- adsorption and the similarity between the SHG data in alkaline and acidic NaF indicates that OH^- adsorption does not exert significant influence on the second order susceptibility of the Ag(111) surface and points to the retention of the negative charge by OH^- upon its adsorption. The latter is in accordance with the conclusions previously made for Ag(111).[11a−c]

The question of whether (partial) charge transfer occurs upon specific anion adsorption on metal surfaces is a controversial issue in interfacial electrochemistry. Frequently, the electrosorption valency, $\gamma = 1/F(\partial\sigma_M/\partial\Gamma)_E$, has been employed as a measure of partial charge transfer. However, the electrosorption valency is a thermodynamic quantity determined by the charge flowing through the interface upon adsorption, and it does not contain information about its microscopic distribution in the interfacial region.[1,26] In the case of chloride and bromide adsorption on Ag single crystals, Guidelli et al.[3g,7b] have proposed that charge transfer to the metal does not occur at lower coverages (at least negative of −0.5 V vs the saturated calomel electrode (SCE) in the case of bromide on Ag(111), corresponding to coverages of up to ~0.25 ML). This was suggested because the ions were not visible by STM and the high mobility was considered a result of weak binding to the substrate.[3g,7b] Theoretical investigations using lattice gas models support this view.[3l,27] Wandlowski et al.[3k] have discussed the effect of screening by the metal and by the solvent for the case of Br adsorption on Ag(100). Screening acts to reduce the surface dipole moment, increasing the electrosorption valency.[3k] Stuve et al. also suggested that water screens coadsorbed chloride ions on Ag(110) surfaces, maintaining a balance between the various interactions between water, chloride, and the metal surface, thus allowing the formation of long-range ordered structures in UHV.[28] Jovic et al. suggested that hydroxide was discharged on Ag(111) and Ag(100) on the basis of a 60 mV shift in adsorption onset potential.[14a] However, the specific adsorption of anions would be expected to depend on the concentration even when not discharged.[11c] Retention of the negative charge by OH^- is in agreement with density functional theory (DFT) calculations,[29] Hartree−Fock calculations,[30,31] and dipped adatom cluster calculations.[17] It is also consistent with the suggestion of Guidelli et al. that charge transfer does not occur for halides at coverages less than ~0.25 ML.[3g,7b]

Ag(110). The Ag(110) anisotropy plots (Figure 10b) show a 2-fold symmetry of two or four maxima. A striking change in the orientation of the symmetry takes place upon an increase of the electrode potential: at the negative and positive potentials, two maxima are present in the same

(24) Richmond, G. L. *Surf. Sci.* **1984**, *147*, 115.
(25) Lee, C. H.; Chang, R. K.; Bloembergen, N. *Phys. Rev. Lett.* **1967**, *18*, 167.
(26) Schultze, J. W.; Rolle, D. *Can. J. Chem.* **1997**, *75*, 1750.
(27) (a) Koper, M. T. M. *J. Electroanal. Chem.* **1998**, *450*, 189. (b) Pacchioni, G. *Electrochim. Acta* **1996**, *41* (14), 2285.
(28) Kizhakevariam, N.; Stuve, E. M.; Dohloelze, R. J. *Chem. Phys.* **1991**, *94* (1), 670.
(29) Koper, M. T. M.; van Santen, R. A. *J. Electroanal. Chem.* **1999**, *472*, 126.
(30) Bagus, P. Unpublished results.
(31) Patrito, E. M.; Parades-Olivera, P. *Surf. Sci.* **2003**, *527*, 149.

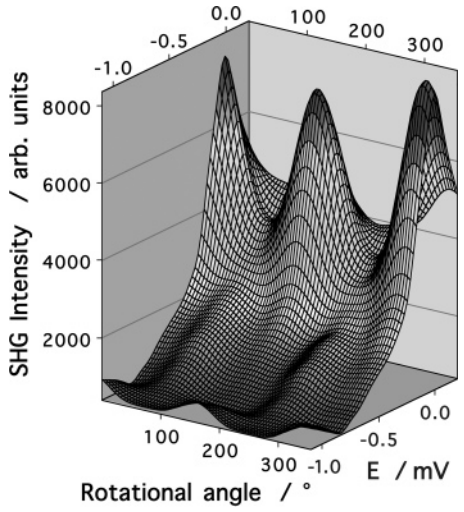

Figure 13. Plot of SH intensity as a function of rotational angle and potential for the Ag(110) surface.

positions, whereas at intermediate potentials, two different maxima are present. From Figure 13, it can be observed that, as the potential is made more positive, two new maxima develop to form four more or less equally sized peaks (at approximately −0.92 V). The two new maxima then develop further until they are larger than the former. As the potential approaches the onset of the current peak labeled B, the former maxima again grow in intensity until four equal maxima are observed at the onset of this current peak (at approximately −0.37 V). At more positive potentials, these maxima continue to grow and the original symmetry pattern is restored. Again, similarly to the behavior exhibited by Ag(111), the most remarkable changes occur upon passing from the potential interval of hydroxide adsorption into the potential region of surface oxide formation.

For the (110) surface, the B and D terms are small and eq 3 reduces to the following:

$$I^{pp}_{SHG} = |A + C\cos 2\phi|^2 = |A|^2 + |C|^2\cos^2 2\phi + 2|A||C|\cos 2\phi\cos\psi \quad (5)$$

where ψ is the phase difference between the A and C terms. Figure 14 displays A, C, and ψ, calculated from fitting the anisotropy results to eq 3, as a function of electrode potential. Some similarities as well as some differences are observed between the SH response from the Ag(110) and Ag(111) planes. The A term again increases along with the electrode potential, showing a close relationship with the charge density. The anisotropic C term for Ag(110) increases with applied potential. This is because the C term contains tensor elements with components parallel and perpendicular to the surface. Thus, it is affected by both the charge density and the symmetry of the surface. At potentials positive of ~0.9 V RPS, both the A and C terms start decreasing, along with the decrease of the current peak and the onset of the current rise. The decrease is likely to be due to the onset of bulk Ag oxidation, as discussed for Ag(111).

At the onset of the current peak labeled B, the A term of the (110) surface exhibits a slightly larger slope versus E than the charge density, whereas for (111) it shows a slope lower than the charge density. This may be related to the different binding sites of atomic oxygen on the different surfaces. It has been proposed that atomic oxygen is preferentially adsorbed in the long bridge sites on

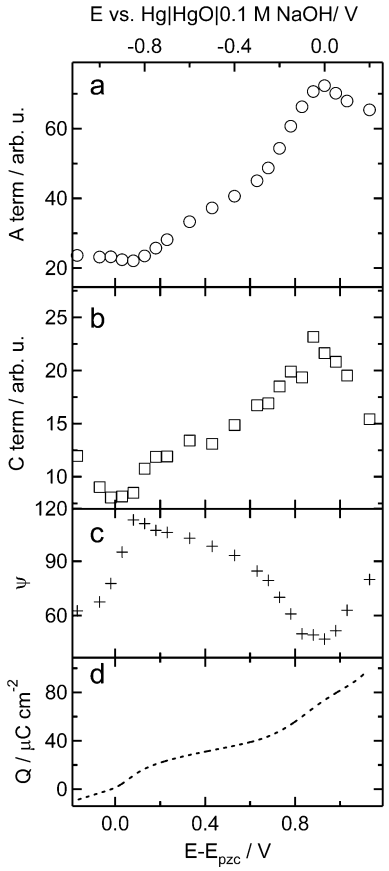

Figure 14. Ag(110) (a) isotropic A term, (b) anisotropic C term, and (c) phase difference (ψ) as a function of electrode potential on the rational scale. Data calculated from anisotropy curves in Figure 13. The dotted line in part d is the charge density.

(110)[22a,32] and in face-centered cubic (fcc) hollow sites on (111).[29,33] Akemann et al. have studied CO adsorption on Pt(111) using SHG and IR spectroscopy and have found that the SH signal was very sensitive to the type of binding site at which CO was adsorbed.[34] This was discussed in terms of different contributions to the SH signal from the different surface dipole moments associated with CO adsorbed at each site. A similar situation may apply in the present case.

The phase for the Ag(110) plane demonstrates rather complex behavior and changes slope three times in the potential interval investigated: at 0.1 V, at around 0.6 V, and at around 0.9 V RPS. Changes in ψ result in strong variation of the anisotropy patterns displayed in Figure 13. From eq 5, it is clear that should ψ pass through 90°, the sign of the corresponding term in the equation would change and effect a reversal in the relative intensities at 0 and 90°. The phase difference between the A and C terms passes through 90° twice: at 0.017 V and at 0.567 V, coinciding with the points at which the SHG symmetry pattern changes. Considering also the scan mode plots, the potentials at which the 0° plot and the 90° plot would converge are the same as those at which cos ψ changes sign.[11d] The change in sign of cos ψ is related to changes in the SH response along the two lattice directions of the surface plane, [1$\bar{1}$0] and [001].[11d] These may be explained by OH^- adsorption along the troughs of the substrate

(32) Pazzi, V. I.; Philipsen, P. H. T.; Baerends, E. J.; Tantardini, G. F. *Surf. Sci.* **1999**, *443*, 1.
(33) Li, W.-H.; Stampfl, C.; Scheffler, M. *Phys. Rev. B* **2002**, *65*, 075407.
(34) Akemann, W.; Friedrich, K. A.; Stimming, U. *J. Chem. Phys.* **2000**, *113* (16), 6864.

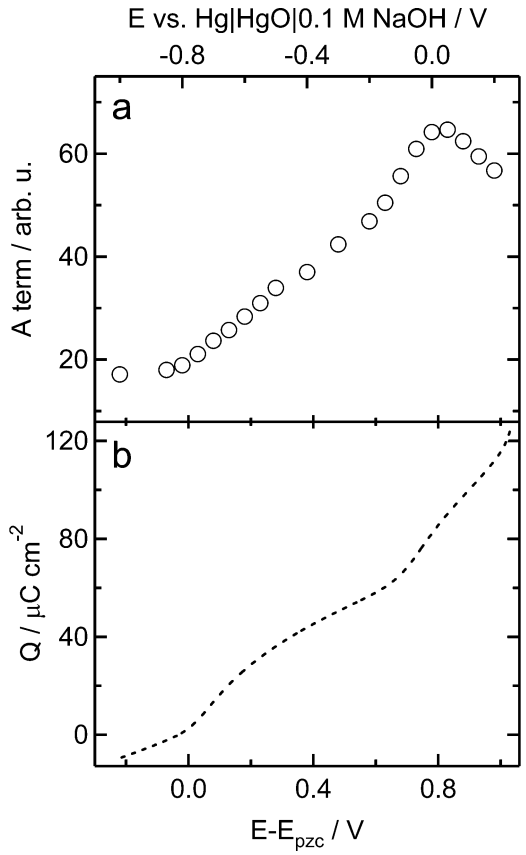

Figure 15. Ag(100) (a) isotropic *A* term as a function of electrode potential on the rational scale. Data calculated from anisotropy curves. The dotted line in part b is the charge density.

surface in the [1$\bar{1}$0] direction, which is evidenced by LEED results (see discussion above and ref 11d).

Differences in the ψ versus potential behavior revealed between the (110) and (111) planes are likely to be related to different adlayer structures. The transition between antiphase domains of $c(2 \times 6)$ symmetry and the ordered $c(2 \times 6)$ adlayer phase takes place at the potential where ψ reaches the maximum (at 0.1 V RPS), and the abrupt change from the $c(2 \times 2)$ structure to the (1×1) phase, corresponding to the transformation from Ag(110)/OH^- to the Ag(110)/O interface, coincides with the second change in ψ, which occurs between ~0.6 and ~0.8 V. Interestingly, for the (110) surface, the changes in ψ are more gradual than those for (111) in this potential interval. The more gradual change in ψ for the (110) surface reflects the shapes of the CVs: the current density rises very sharply for (111) and rises more gently to form a rounded peak for (110). The distinct changes in ψ observed in the presence of OH^- at the onset of the second current peak point to a substantial change in the electronic structure of the interface upon formation of the surface oxide.

Ag(100). The Ag(100) surface displayed no symmetry pattern. This result is expected because the 4-fold contribution to the symmetry can only arise from bulk terms in the SH response, which is forbidden in the dipole approximation. In fact, the SH response from the bulk for all surface symmetries has been reported to be substantially smaller than that from the surface (top one or two layers of metal atoms).[9a,c,35] The *A* term calculated from the anisotropy data is plotted in Figure 15. The negligible anisotropy of the (100) plane reduces the amount of useful information obtained upon studying this surface with SHG. The *A* term of the (100) surface behaves similarly to that of the Ag(110) plane. It follows the increase in the charge density linearly in the potential interval of the first voltammetric peak labeled A and then increases faster than the charge. At 0.85 V RPS, where the current corresponding to bulk Ag oxidation sets in, the *A* term starts to decrease.

(35) Guyot-Sionnest, P.; Chen, W.; Shen, Y. R. *Phys. Rev. B* **1986**, *33*, 8254.

4. Summary and Conclusions

Cyclic voltammograms for the three low index Ag crystal faces in alkaline NaF/NaOH electrolyte are compared for the first time. The voltammograms show a high degree of reversibility in the potential interval below bulk Ag_2O formation and are attributed to the specific adsorption of hydroxide followed by surface oxide formation. The differences in the positions of the voltammetric peaks and their profiles for Ag crystal planes are explained by different (i) work functions, (ii) surface atomic densities, and (iii) corrugation potentials for these surfaces.

LEED and RHEED measurements demonstrate that the different corrugation potentials of the surfaces give rise to different adsorption characteristics of OH^-: on the (110) plane, ordered structures are produced, whereas, on the (100) and (111) planes, disordered overlayers are formed. Upon transformation of Ag/OH to Ag/O, disordered surface oxide phases are formed, although RHEED shows that some small islands of $c(2 \times 2)$ structure are present on the (110) surface and, at more positive potentials, on (100).

Second harmonic generation (SHG) measurements were performed (i) in the potential scan mode at constant rotational angle and (ii) at constant potential as a function of the rotational angle. The isotropic *A* terms (for the (111), (110), and (100) planes), anisotropic (2-fold *C* for the (110) plane and 3-fold *D* for the (111) plane) terms, and the phase difference (ψ) (between the *A* and *C* terms for (110) and the *A* and *D* terms for (111)) were calculated by fitting the experimental data. Comparison of the data for the three Ag single-crystal planes shows that the most pronounced changes in the SH response occur upon transformation of the specifically adsorbed hydroxide adlayer into surface Ag_2O oxide and later on into bulk Ag(I) oxide. The transformation of Ag/OH into Ag/O is characterized by pronounced changes in ψ for Ag(111) and Ag(110) and a change in the slope of *A* versus the potential for Ag(100). The onset of bulk Ag oxidation is marked by a drop of the isotropic contribution to the SH intensity for all three planes due to the lower polarizability of an oxide-covered surface compared with a metal surface. The SH intensity appears to be very sensitive to the early steps of the oxidation process and starts declining when the charge transferred through the interface reaches 0.5–0.6 e^- per surface Ag atom. In the hydroxide adsorption region, the isotropic contribution for all three surfaces increases with potential, roughly following an increase of the charge on the surface. For Ag(111), no changes in ψ occur in the OH^- adsorption region, which is consistent with an absence of extended ordered adsorbate structure (as revealed by LEED). Contrary to that, Ag(110) exhibits changes in ψ at potentials corresponding to the transitions between different Ag/OH^- adlayer structures. LEED and RHEED and in situ SHG have proved to be a useful combination for studying the electrochemistry of Ag surfaces in alkaline solutions.

In conclusion, we would like to stress that SHG is an in situ technique, which is highly sensitive to the electron distribution at the interface and the symmetry of the

topmost layers of the surface, and it has the further advantage that a thin layer configuration is not required. It is thus rather unfortunate that a lack of theoretical understanding limits the information that can be extracted upon application of SHG to electrified interfaces. It is our hope that this work will stimulate further studies in the theory of SHG from solid/liquid interfaces so that the full potential of this technique can be realized.

Acknowledgment. Financial support from the European Union 5th Framework program (Contract No. HPMF-CT-2000-00955) (S.L.H.) and from the Max Planck Gesellschaft (S.L.H., A.L.N.P., and E.R.S.) is gratefully acknowledged. The authors also express their thanks to Dr. K. Doblhofer and Dr. E. Santos for interesting and helpful discussions and for providing useful references, to Dr. A. Scheybal for advice on UHV silver single-crystal preparation, and to Mr. R. Putzke and Mr. P. Tesky for their expertise in the design and construction of the electrochemical cell.

LA0483818